Eur. Phys. J. A (2020) 56:269
https://doi.org/10.1140/epja/s10050-020-00281-y

THE EUROPEAN PHYSICAL JOURNAL A

Regular Article - Experimental Physics

Measurement of electric quadrupole moment in neutron rich ^{131,132}I

S. S. Alam[1,2], D. Banerjee[2,3], T. Bhattacharjee[1,2,a], P. Blaha[4], D. Kumar[1,2], A. Saha[1,7], M. Saha Sarkar[5], S. Sarkar[6], S. K. Das[3]

[1] Variable Energy Cyclotron Centre, Kolkata 700 064, India
[2] Homi Bhabha National Institute, Anushakti Nagar, Mumbai 400 094, India
[3] RCD-BARC, Variable Energy Cyclotron Centre, Kolkata 700 064, India
[4] Institute of Materials Chemistry, Vienna University of Technology, Wien 1060, Austria
[5] Saha Institute of Nuclear Physics, Kolkata 700 064, India
[6] Indian Institute of Engineering Science and Technology, Shibpur, West Bengal 711 103, India
[7] Present Address: ICFAI University, Agartala, Tripura 799210, India

Received: 12 May 2020 / Accepted: 13 October 2020

Communicated by Wolfram Korten

Abstract The quadrupole moments of the excited levels in neutron rich iodine isotopes, viz., ^{131}I ($5/2^+_1$) and ^{132}I (3^+_1), have been measured with $LaBr_3$(Ce) detectors using Time Differential Perturbed Angular Correlation (TDPAC) spectroscopy. The excited levels were populated from β^- decay of the radiochemically separated tellurium (Te) fission products produced in ^{nat}U(^{4}He,f) reaction at E_α(lab) = 40 MeV from K-130 cyclotron at VECC, Kolkata. The active tellurium fission products were radiochemically doped in metallic tellurium matrix to provide the necessary Electric Field Gradient (EFG) required for TDPAC measurement. The values of quadrupole moments for the $5/2^+_1$ level of ^{131}I and 3^+_1 level of ^{132}I were determined to be $(-)0.30(1)$ eb and $(-)0.25(2)$ eb, respectively. The present measurement provides the first experimental determination on the electric quadrupole moment of $5/2^+_1$ level of ^{131}I.

1 Introduction

The measurement of electric quadrupole moment is important to estimate the deviation of the nuclear charge distribution from sphericity [1,2]. It is also a sensitive probe to indicate the evolution of shell structure. Thus, such measurements in neutron rich nuclei below doubly closed ^{132}Sn are of substantial importance to probe the prevalence of expected spherical character as one approaches the N = 82 shell closure in this exotic domain [3–5]. However, the availability of experimental data on electric quadrupole moments (EQM) in this mass region are inadequate. Apart from a few, most of the existing results are from measurements done during early 60s to late 80s [6]. So, it is important to perform more measurements on electric quadrupole moment to enrich the understanding of the evolution of shell structure around ^{132}Sn.

In case of iodine nuclei, the systematic change of measured EQM for the $5/2^+_1$ and $7/2^+_1$ levels were studied in 1964 [7]. It was found by the authors of Ref. [7] that a linear extrapolation of the measured values to the closed neutron shell at N = 82 predicted a value of Q = 0.11 b for the $7/2^+_1$ state. However, the extrapolated value of EQM for $5/2^+_1$ state, obtained in a similar manner, is much larger. In contrast to the data, both the theoretical calculations performed at that time, (i) by Kisslinger and Sorensen [8] and (ii) the single-particle estimates and the configuration mixing calculations by Horie and Arima [9], predicted a larger absolute value of EQM for $7/2^+_1$ level compared to that for $5/2^+_1$ level in N = 82 iodine nucleus.

It is worth mentioning that in Ref. [7], specifically for the $5/2^+_1$ level, the linear extrapolation was based on only three data points which are again significantly away from shell closure of N = 82. So, systematic experimental determination of quadrupole moments up to N = 82 iodine is of importance to understand the evolution of nuclear deformation of the $5/2^+_1$ and $7/2^+_1$ levels. Subsequent to the work of Ref. [7], very few measurements of EQMs of iodine nuclei have been performed [10–13]. Till date, no experimental measurement exists on the EQM of $5/2^+_1$ levels in odd-A iodine with $N > 76$.

S. K. Das: Retired.

[a] e-mail: btumpa@vecc.gov.in (corresponding author)

Published online: 22 October 2020

In the present work, the quadrupole moment for the $5/2_1^+$ level of $N = 78$ ^{131}I has been measured with latest generation $LaBr_3$(Ce) scintillator detectors using TDPAC spectroscopy [14]. The TDPAC measurement was performed with iodine as PAC probe doped in metallic tellurium matrix. The active iodine isotopes were produced from the β-decay of respective tellurium parent isotopes. The neutron rich tellurium isotopes were produced by the α induced fission of ^{nat}U followed by their radiochemical separation from the rest of the fission products. The tellurium isotopes were doped into the tellurium metal during the radiochemical separation process to provide the necessary Electric Field Gradient (EFG) to interact with the EQM of the nuclear states. The quadrupole moment of 3_1^+ level of ^{132}I produced from decay of ^{132}Te, which had sufficient activity in the prepared sample, was also measured. This is, however, was measured earlier [12,15] by Integral Perturbed Angular Correlation (IPAC) technique that usually introduces larger uncertainties compared to the TDPAC method. So, the present work provides the first experimental result on the quadrupole moment of the $5/2_1^+$ level in odd-A iodine above N = 76 and that of the 3_1^+ level of ^{132}I using a different technique.

2 Methods and materials

The determination of EQM of an excited nuclear state relies on the direct or indirect measurement of its interaction with an EFG. The EFG produced at the site of the nucleus due to the presence of surrounding charges in an atomic or molecular environment could be sufficient to yield a measurable effect by interacting with the nuclear charge distribution. In case of a solid, an EFG $\sim 10^{21}$ V/m^2 can be obtained from the periodically arranged atomic or molecular charges present around the nucleus. The interaction between the EQM of an excited state of the nucleus and the EFG can be measured by a hyperfine technique, viz., TDPAC Spectroscopy [14]. In a TDPAC experiment, the time differential perturbation in the $\gamma-\gamma$ angular correlation, arising due to such kind of electric quadrupole interaction, is measured to determine the electric quadrupole moment of the nuclear excited state.

The following two subsections describe the production of neutron rich iodine isotopes and the TDPAC technique used for the measurement of EQM in the present work.

2.1 Production of ^{131,132}I and sample preparation

The excited states of ^{131,132}I have been populated from the β^- decay of ^{131m}Te ($t_{1/2} \sim 33$ h) and ^{132}Te ($t_{1/2} \sim 3$ d), respectively. The parent nuclei were produced via ^{nat}U(^4He, f) reaction followed by radiochemical separation. Stacks of $\sim$1 mg/cm^2 thick ^{nat}U targets, prepared by electro-deposition on 25 μm thick Aluminium backing foil, was irradiated with 40 MeV α beam for 36 h at K = 130 AVF cyclotron of VECC, Kolkata. Each stack was prepared with four / five Uranium targets separated by 25 μm thick Aluminium catcher foils. The recoiling fission products were collected on the catcher foils which were subsequently used for the radiochemical separation and doping into tellurium metal matrix. In order to separate the tellurium isotopes from rest of the fission products, the catcher foils were dissolved in concentrated nitric acid followed by the addition of inactive tellurium carrier. The radioactive tellurium along with the tellurium carrier were reduced to metallic Te(0) by chemical method. The metallic tellurium was then annealed at 573 K for 3 h in argon atmosphere. The crystalline phase of the metallic tellurium powder, prepared in this way, was of near spherical shape with $\sim$5 mm diameter and was characterized by powder X-ray Diffraction (XRD) measurement. All the peaks obtained in XRD analysis could be assigned to the trigonal crystal structure of tellurium metal powder.

2.2 TDPAC method

In the TDPAC technique [14], the perturbation in the angular correlation of a $\gamma-\gamma$ cascade, created by the interaction of the electric quadrupole moment of the intermediate state with the known EFG (V_{zz}) around the probe atom, is utilized for the measurement of nuclear quadrupole moment (Q). As a result of the perturbation, the intermediate state is split into different non-degenerate m-states with eigen values proportional to the quadrupole frequency ω_Q which is given by:

$$\omega_Q = \frac{eQV_{zz}}{4J(2J-1)\hbar} \tag{1}$$

where J is the spin of the intermediate level. The spin independent quadrupole interaction frequency coupling constant (ν_Q) can be derived as

$$\nu_Q = \frac{eQV_{zz}}{h} \tag{2}$$

Due to the above interaction, the angular correlation function is perturbed by a time dependent factor known as the perturbation factor $G_2(t)$.

The theoretical shape of $G_2(t)$ for static electric field gradient (EFG) in a polycrystalline powder sample is given by the following equation [16]:

$$G_2(t) = a_0 + \sum_n a_n \cdot e^{(-\omega_n \delta t)} \times e^{(-\frac{1}{2}\omega_n^2 \tau_R^2)} \times cos(\omega_n t) \tag{3}$$

The summation index "n" can assume all positive integer values (including zero) and its maximum value depends on the number of hyperfine split levels. The exponential damping

terms in Eq. (3) attribute to (i) the finite resolving time (τ_R) of the measurement setup, characterized by a Gaussian distribution and (ii) the inhomogeneity introduced during sample preparation, expressed with the Lorentzian frequency distribution having relative width parameter δ. The coefficients a_n have dependence on the nuclear radiation parameters and the electric field asymmetry parameter $\eta = \frac{|V_{xx}-V_{yy}|}{V_{zz}}$. As evident from the above equation, the theoretical shape of the perturbation function is significantly affected by instrumentation, asymmetry of EFG and quality of the sample along with the population mode of the $\gamma - \gamma$ cascade, as follows.

(1) Firstly, because of the intrinsic time resolution of the coincidence circuit and with the approximation that the resolution function is a Gaussian distribution of width τ_R, a correction factor $e^{(-\frac{1}{2}\omega_n^2\tau_R^2)}$ is introduced into the expression given in Eq. (3). The multiplication with this correction factor attenuates the amplitude of oscillations and shifts the zero time from its true value. (2) The second effect arises from a situation where the EFG has no axial symmetry ($\eta \neq 0$), i.e from the asymmetry η of EFG. The eigen values of the m states are approximated by power series of η and the transition frequencies become η-dependent with the loss of harmonic nature of quadrupole frequency (with exception for $\eta = 1$). (3) The third effect originates from the inhomogeneity of polycrystalline solid and defects present in that sample. This effect may result in situations where the crystalline fields experienced by the nucleus in its intermediate state vary considerably from nucleus to nucleus. So, the experimental curve is fitted with a distribution of frequencies.

Experimentally, the $\gamma - \gamma$ coincidence histograms, given by $W(\theta, t) = \sum A_k.G_k(t).P_k(cos\theta)$, are recorded as a function of time elapsed between the emission of feeding and decaying γ-rays, at all possible 90° and 180° angles. The experimental perturbation function $G_2(t)$, obtained with Eq. (4), is least-square fitted with the theoretical expression to get the hyperfine parameters ν_Q and η.

$$A_2.G_2(t) = 2 \times \frac{W(180°, t) - W(90°, t)}{W(180°, t) + 2W(90°, t)} \quad (4)$$

As the quadrupole coupling constant, ν_Q, is proportional to the EQM (Q) and EFG (V_{zz}), EQM is directly obtained knowing the EFG which is discussed in Sect. 3.1.

In the present experiment, performed at room temperature, the separated tellurium fission fragment activity doped in tellurium metal was counted using BGO suppressed Clover HPGe detectors prior to the TDPAC measurement in order to identify the γ lines of interest and their coincidence relationships with other observed γ rays. The TDPAC spectrometer consisted of three 1 inch $\phi \times 1$ inch thick cylindrical $LaBr_3$(Ce) crystals coupled to XP2020URQ Photomultiplier tubes and kept in a planar geometry. One of the detectors was used as the 'START' detector and the other two as 'STOP-90' and 'STOP-180' detectors based on their angular position of 90° and 180°, respectively, with respect to the 'START' detector. The tellurium powder sample was kept at a distance of 5 cm from the detectors for counting. The distance was chosen in such a way that the geometrical correction due to cylindrical detectors is minimum and coincidence count rate is maximum with the available source strength [17]. The typical activity was 10–20 μCi depending on the number of Uranium targets used in the stack and the beam current provided for irradiation. The data were collected in LIST mode with the help of standard NIM and CAMAC electronics. The energy spectra from the $LaBr_3$(Ce) detectors are displayed with a range of 600 keV and the time spectra corresponding to two STOP detectors are displayed in a total range of 500 ns, both in 8K channels. The typical energy resolution of the detectors used in the setup is ~3% at 662 keV γ energy. The Full Width at Half Maxima (FWHM) of the prompt coincidence time peak obtained with the TDPAC setup at the relevant energies are discussed in Sect. 3.2. The statistics was gathered by repeating the irradiation, sample preparation and TDPAC counting several times in sequence.

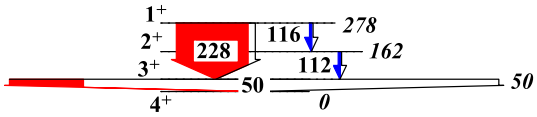

Fig. 1 The simplified decay scheme for ^{132}I, as populated from the decay of ^{132g}Te. The γ rays of interest in the measurement of EQM are shown in red. The two other γ rays are shown in blue. The conversion coefficents have been used while showing the intensities of the γ lines (proportional to the width of the transitions) and the converted intensity is indicated with the white portion in the width of the transition. The data has been taken from ENSDF [18]

3 Experimental results

The simplified decay schemes of the two nuclei, viz. ^{132}I and ^{131}I [18,19], as obtained from the decay of respective tellurium parents are shown in Figs. 1 and 2. In these figures, the cascade relevant to the TDPAC analysis is shown in red, the γ rays (< 600 keV) expected in the energy spectrum are shown in blue and the higher energy γ rays are shown in black. The determination of EFG and EQM are described in the following two subsections.

3.1 Determination of EFG

In the present case, the EFG at the iodine site in tellurium matrix has been obtained from the experimental data available in literature. The EFG for this system can be esti-

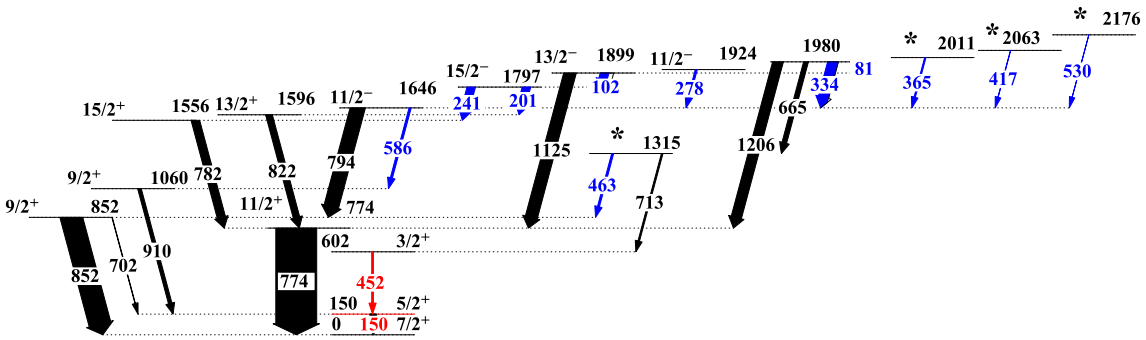

Fig. 2 The simplified decay scheme for ^{131}I, as populated from the decay of ^{131m}Te and relevant in the present measurement. The γ rays of interest in the measurement of EQM are shown in red. The γ rays with energy below 600 keV are shown in blue and the higher energy γ rays are shown in black. The conversion coefficents have been used while showing the intensities of the γ lines (proportional to the width of the transitions) and the converted intensity, if any, is indicated with the white portion in the width of the transition. The data has been taken from ENSDF [19]. The J^{π} of the levels are adopted from Ref. [20]. The levels marked with * have uncertain J^{π} which are not shown

Table 1 The EFG values obtained for iodine in tellurium(Te) with known values of quadrupole frequencies and quadrupole moments (Row 1–3). (**a**): The EFG value is quoted as given in Ref. [12]. (**b**): Represents the V_{zz} obtained with scaling the EFG of Row 4 with the latest value of quadrupole moment [23]. See text for details

Nucleus and Host	Nuclear spin (J^{π})	ν_Q(MHz)	T(K)	Q(eb) [23]	V_{zz}(V/cm^2)
^{127}I in Te	$7/2^+_1$	693(200) [21]	293	−0.617(2)	$4.65(134) \times 10^{18}$
^{129}I in Te	$7/2^+_1$	396(3) [21]	4.2	−0.483(10)	$3.39(7) \times 10^{18}$
^{129}I in Te	$7/2^+_1$	406(6) [22]	80	−0.483(10)	$3.48(9) \times 10^{18}$
^{129}I in Te	$7/2^+_1$	406(6) [22]	300	−0.553(10)	$3.38(4)\times 10^{18}$ (*a*)
^{129}I in Te	$7/2^+_1$	406(6) [22]	300	−0.483(10)	$3.87(12)\times 10^{18}$ (*b*)

mated using the known quadrupole frequencies [21,22] and quadrupole moments [23] for the $7/2^+_1$ states of ^{129}I and ^{127}I that are shown in Row 1–3 of Table 1. In addition, the EFG value for iodine site in tellurium matrix has also been taken from Ref. [12] that was obtained from the data of $7/2^+_1$ state of ^{129}I considering Q = −0.553(10) eb (Row 4 of Table 1). Further, this value of EFG ($3.38(4)\times 10^{18}$ V/cm^2) has been scaled with the latest quadrupole moment for this level reported in Ref. [23]. The scaled EFG comes out to be $3.87(12)\times 10^{18}$ V/cm^2 (Row 5 of Table 1).

From the values shown in Table 1, it is observed that there is no considerable change in the EFG value as a function of temperature. Out of the obtained values, the value shown in Row 1 suffers from a large (∼ 30%) error and was not considered for subsequent extraction of quadrupole moments in the present work. The value shown in Row 5 is also not considered as this goes against the expected trend of EFG as a function of temperature. The values shown at Row 2 and 3 are found to be similar within their errors. Subsequently, the EFG value of Row 2 ($3.39(7) \times 10^{18}$ V/cm^2), consequent to its lower error value, was used for the determination of quadrupole moments for ^{131,132}I.

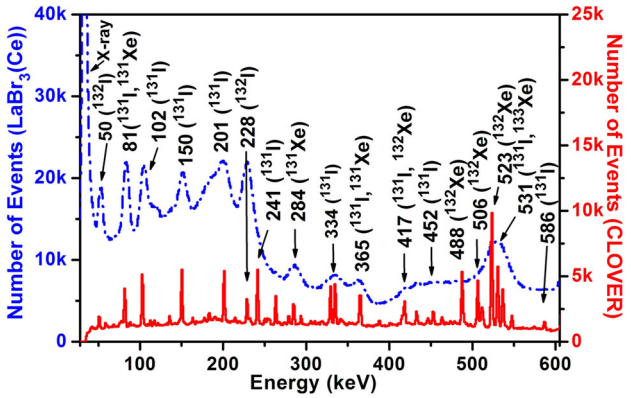

Fig. 3 The representative total projection obtained with the BGO suppressed Clover HPGe and the $LaBr_3$(Ce) detectors are plotted. The comparison clearly identified the photopeaks required for the subsequent TDPAC analysis and other γ peaks that are generated from the decay of radio-chemically separated tellurium activity

3.2 Determination of EQM using TDPAC method

The γ energy spectra obtained with the tellurium metal sample doped with active ^{131,132}Te, using Clover HPGe and $LaBr_3$(Ce) detectors, are shown in Fig. 3. The comparison of these two spectra has helped in identifying the required

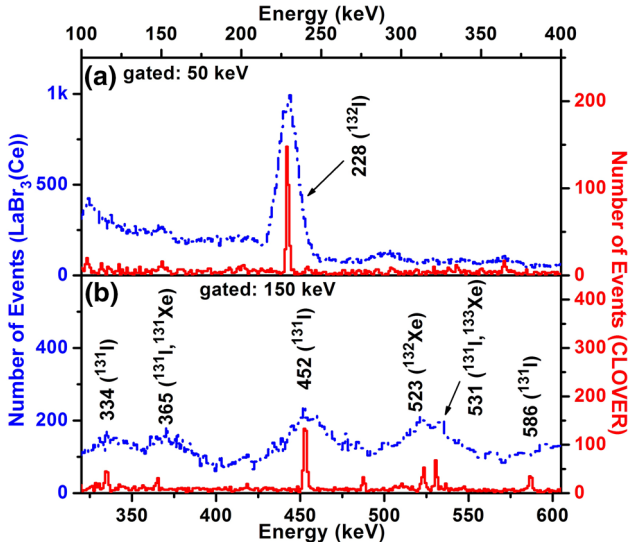

Fig. 4 The representative gated projections are shown for (**a**) 50 keV and (**b**) 150 keV, obtained from the data taken with Clover HPGe and the $LaBr_3$(Ce) detectors, respectively, corresponding to the 228–50 keV and 452–150 keV cascades of ^{132}I and ^{131}I, respectively. These projections were used for the generation of coincidence time spectra with $\gamma - \gamma$ energy ('START-STOP') gating in two $LaBr_3$(Ce) detectors. The close lying contamination peaks from the daughter products, that might arise from the coincidence with underlying Compton background, are also marked

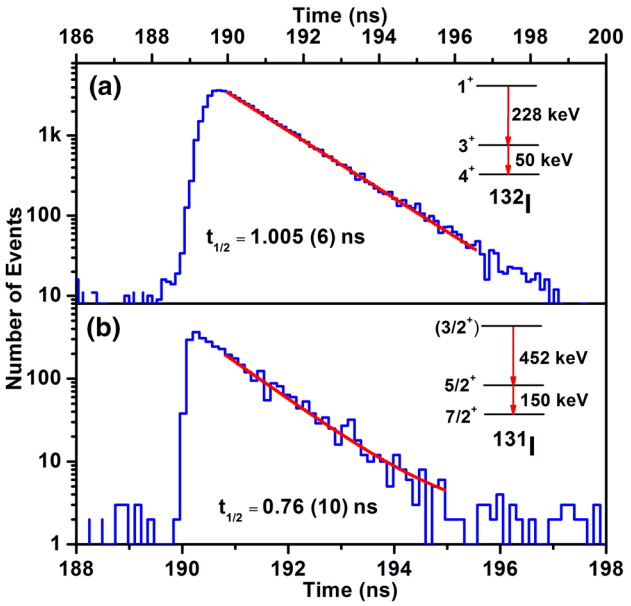

Fig. 5 The representative background subtracted time projections are shown for (**a**) 228–50 keV and (**b**) 452–150 keV, respectively, obtained from the data taken with the TDPAC setup. The time values in the X-axis is the time difference measured with the TAC module having a total range of 500ns. The feeding transitions were selected from the 'START' detector and the decaying transition from the 'STOP' detectors of the setup

γ transitions and cascades for subsequent analysis. The relevant cascades connecting the levels of interest and other expected γ rays are visible in this spectrum which corroborate with the simplified decay schemes displayed in Figs. 1 and 2. The difference in the Clover and $LaBr_3$(Ce) spectra may be attributed to the difference in coincidence time window used for generation of the spectra, the difference in attenuation in the entrance windows of the detectors and the applied CFD (Constant Fraction Discriminator) thresholds. The quadrupole moment measurements were performed for the 50 keV, 3_1^+ level of ^{132}I ($t_{1/2}$ = 1.120(15) ns [24]) and 150 keV, $5/2_1^+$ level of ^{131}I ($t_{1/2}$ = 0.95(5) ns [19]), respectively, using TDPAC technique described under Sect. 2.2. The energy projections from $LaBr_3$(Ce)-$LaBr_3$(Ce) coincidences, corresponding to the two cascades of interest, are shown in Fig. 4 and compared with that obtained from Clover-Clover coincidences.

The time spectra were generated from double coincidence data in two $LaBr_3$ ('START' and 'STOP') detectors by selection of narrow energy gates corresponding to the 228–50 keV and 452–150 keV cascades, respectively. The feeding transition was selected with the 'START' and the decaying transition was selected with the 'STOP' detector while generating the time spectra. The chance coincidences present in the time spectra, if any, was found by gating on the Compton background just near the photo-peak and subtracted appropriately. A set of representative time spectra for the two relevant cascades of ^{132}I and ^{131}I are shown in Fig. 5 along with the measured halflives that were obtained by fitting the observed slope. The correctness of the time spectra was ensured by comparing the measured halflives with the known values available in literature. In the present work, the halflives for the 3_1^+ level of ^{132}I and the $5/2_1^+$ level of ^{131}I come out to be 1.005(6) ns and 0.76(10) ns, respectively. During analysis, the FWHM of the prompt concidence peak at relevant energies were also obtained from the prompt time curves generated using ^{106}Ru source and selecting the energies from the Compton profile of the spectra from 'START' and 'STOP' detectors. These values were found to be 567(6) ps and 386(8) ps, for the 228–50 keV cascade of ^{132}I and 452–150 keV cascade of ^{131}I, respectively. The time spectra generated with the complete data set was used for the subsequent TDPAC analysis.

The TDPAC spectra ($A_2G_2(t)$ vs Time), obtained for the 50 keV level of ^{132}I and 150 keV level of ^{131}I, have been shown in Fig. 6 using the 228–50 keV and 452–150 keV cascades, respectively, along with their corresponding Fourier transforms (FT). The fitting of the experimental data points was performed for a time interval of 7 ns. A Kaiser-Bessel window function [25] was used to generate the Fourier transform. This window function was used to reduce the side lobes around the central peak. The fitted parameters were obtained based on the condition to obtain a minimum χ^2 value for least square fitting.

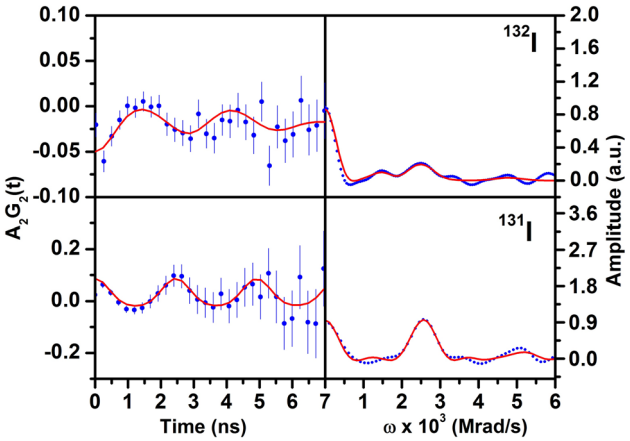

Fig. 6 TDPAC spectra (left) and their Fourier transforms (right) for the 50 keV, 3_1^+ level of ^{132}I and 150 keV, $5/2_1^+$ level of ^{131}I, respectively. The blue circles correspond to the experimental data and the red solid lines represent the fitting

The unperturbed angular correlation coefficient (A_2) for the 228–50 keV cascade of ^{132}I comes out to be -0.05(1) in the present work and it is in reasonable agreement with the earlier measured value of -0.042(10) [26]. For the 452–150 keV cascade of ^{131}I, the experimental value of +0.08(2) is slightly higher than the previously observed value of + 0.058(8) [27]. The deviation from the theoretical unperturbed angular correlation coefficients, viz. − 0.0714 for 1-E2-3-M1-4 cascade of ^{132}I and 0.05 for 3/2-M1-5/2-M1-7/2 cascade of ^{131}I, could be due to even very small mixing of higher multipoles in the associated γ transitions. For ^{132}I, both the 50 keV (M1) and 228 keV (E2) transitions are known as pure multipoles [18]. An E2 mixing of $\sim$ 0.09% in the 50 keV transition ($\delta_m = -0.03$, δ_m is mixing ratio) and a pure E2 nature of 228 keV transition explains the observed anisotropy in the present work. In case of ^{131}I, both the 150 keV and 452 keV transitions are known as mixed as per the conversion electron measurement [28]. In this measurement, the 150 keV transition was shown to have a multipole mixing of M1 (90%) + E2 (10%) and the 452 keV as mixed M1 + E2 transition. It is found that a mixing of $\sim$ 1.4% of E2 in 452 keV ($\delta_m = +0.12$), in addition to the 10% E2 mixing ($\delta_m = +0.33$) in 150 keV, explains the observed anistropy for this cascade.

During the data analysis, the asymmetry parameter η was kept as 0.73(2) [22] for both ^{131}I and ^{132}I, following the good precision obtained in the Mössbauer spectroscopy data with iodine nucleus in tellurium matrix. In the analysis, the ω_Q is found from the combination of all the transition frequencies among the different hyperfine states. Hence, the difference in ω_Q values for ^{131}I (J = 5/2) and ^{132}I (J = 3) is due to the spin of the intermediate state as well as the non-zero η value. The uncertainty in the frequency determination has been obtained while least-square fitting of the experimental data with theoretical function (Eq. 3) through χ^2 optimization that has to take into account the correlations among different parameters including the inhomogeneity parameter δ. The inhomogeneity parameter δ was varied and finally fixed at 10% that was found to give the best χ^2 value and lowest error for the quadrupole frequency. The values of quadrupole coupling constant (ν_Q) were derived from ω_Q values obtained from the fitting and are tabulated in Table 2 along with the other relevant parameters like excitation energy (E_x), spin-parity (J^π), level halflife ($t_{1/2}$) and the EFG (V_{zz}).

Taking the values of V_{zz} (EFGs) as $3.39(7) \times 10^{18}$ V/cm^2 (as shown in Row 2 of Table 1), the quadrupole moment of 50 keV state of ^{132}I ($J^\pi = 3_1^+$) and that of 150 keV state of ^{131}I ($J^\pi = 5/2_1^+$) are extracted and shown in Table 2. The quadrupole moment of the 3_1^+ level of ^{132}I was found to be (−)0.25(2) eb which is in close agreement with the earlier works [6,12,15]. The extracted quadrupole moment for the $5/2_1^+$ level in ^{131}I comes out to be (−)0.30(1) eb that gives the first experimental data for this level. The errors quoted for the EQM are calculated from the error in quadrupole frequency and the error in the experimental EFG values. As the TDPAC method is not capable of determining the sign of the quadrupole moment, negative sign has been adopted following the systematics and the same have been quoted in Table 2 as well as in all the subsequent discussions.

4 Discussion

The electric quadrupole moments of the 150 keV, $5/2_1^+$ level of ^{131}I and 50 keV, 3_1^+ level of ^{132}I, measured in the present work, have been compared with the data in the neighboring nuclei and are used to study the evolution of collectivity in the odd-Z, odd-A nuclei around ^{132}Sn. In addition, a large basis shell model calculations have been performed to interpret the present experimental data. The evolution of collectivity and the shell model interpretations are discussed in the following two subsections.

4.1 Evolution of collectivity

In order to understand the evolution of collectivity from the measured quadrupole moments of the first $5/2^+$ and the $7/2^+$ levels of iodine nuclei up to N = 82, the known quadrupole moments for these levels, including the one measured in the present work, are plotted as a function of neutron number (N) in Fig. 7. In this plot, the maximum and minimum values of quadrupole moments, known for a particular level, have been taken from the IAEA compilation [15] along with the adopted values from Ref. [6]. This shows that, although the quadrupole moments of the $7/2_1^+$ levels in odd-A iodine nuclei show a linear dependence on neutron number from N = 74–80 (dotted black line of Fig. 7a), the quadrupole moments

Table 2 The values for V_{zz}, ω_Q and Q-mom, obtained in the present work for the first excited levels of ^{131,132}I. The sign of the EQM could not be determined in the present experiment and the negative signs are adopted following the systematics

Nucleus	E_x (keV)	J^π	Cascade (keV)	$t_{1/2}$ (ns)	V_{zz} (V/cm^2)	ν_Q (MHz)	Q-mom. (eb)		
							Pres. work	Ref. [12]	Refs. [6,15]
^{132}I	50	3^+_1	228–50	1.005(6)	$3.39(7) \times 10^{18}$	204(16)	(−)0.25(2)	(−)0.23(7)	(−)0.20(6)
^{131}I	150	$5/2^+_1$	452–150	0.76(10)	$3.39(7) \times 10^{18}$	247(6)	(−)0.30(1)	–	–

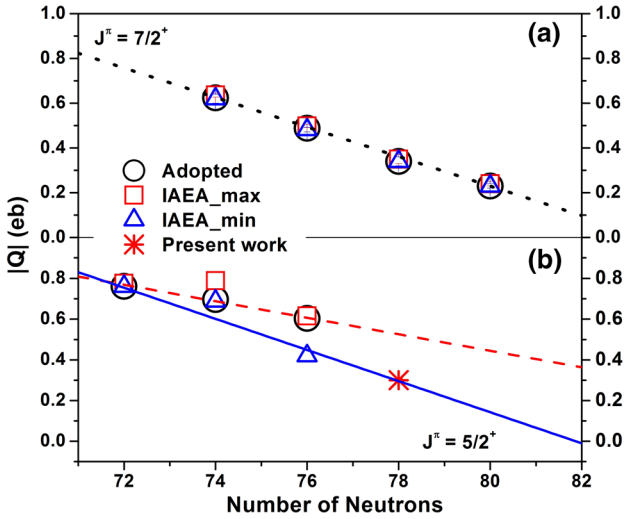

Fig. 7 Experimental quadrupole moments (magnitude) for the (**a**) $7/2^+_1$ and (**b**) $5/2^+_1$ levels of odd-A I are shown as function of neutron number. The adopted values of quadrupole moments have been taken from Ref. [6], the maximum and minimum values, known for a particular isotope, have been taken from the IAEA compilation [15]. Errors have been considered but not visible in some cases as the corresponding error bars are smaller than the size of the symbol used. The value at N = 78 for the $5/2^+_1$ level of ^{131}I is measured in the present work and is shown. Linear extrapolations up to N = 82 are shown for $7/2^+$ level (black dotted line) and $5/2^+$ level (red dashed and blue solid lines) with different data sets. See text for details

of the $5/2^+_1$ levels depict a different scenario. Grossly, the quadrupole moments of the $5/2^+_1$ levels of odd-A iodine nuclei display not so linear dependence on the neutron number. However, it might be noticed that two different linear extrapolations are quite possible with different sets of data available for this level.

The adopted values for the $5/2^+_1$ levels from N = 72 to 76 follow a particular linear dependence on neutron number (dashed red line in Fig. 7b) that was considered in Ref. [7]. The corresponding linear extrapolation up to N = 82 predicted a higher value of quadrupole moment for the $5/2^+_1$ level than that for the $7/2^+_1$ level (∼ 0.1 eb). However, a different slope for the linear extrapolation is obtained considering the adopted value at N = 72, the lowest value at N = 76 and the value at N = 78 that is measured in the present work (solid blue line in Fig. 7b). This latter exrapolation also provides a lower value of quadrupole moment at N = 82 for the $5/2^+_1$ level compared to that for the $7/2^+_1$ level. The single particle estimates [9] for N = 82 iodine comes out to be −0.217 eb for $7/2^+_1$ level and -0.185 eb for the $5/2^+_1$ level. For the calculation, the configurations of $\pi g^1_{7/2}$ (J = 7/2) and $\pi d^1_{5/2}$ (J = 5/2), respectively, have been considered for the $7/2^+_1$ and $5/2^+_1$ levels.

In order to understand the global scenario on the evolution of deformation for the first $5/2^+$ levels in the odd-Z, odd-A nuclei around ^{132}Sn, the deformation parameter (β_2) has been extracted from the measured quadrupole moments (Q_s) using Eqs. (5) and (6) given below.

$$Q_0 = Q_s \frac{(2J+3)(J+1)}{3K^2 - J(J+1)} \tag{5}$$

$$\beta_2 = \frac{\sqrt{5\pi}}{3ZR^2} Q_0 \tag{6}$$

where Q_0 is the intrinsic quadrupole moment, K is the component of spin (J) along the intrinsic symmetry axis, $R = R_0.A^{1/3}$ and $R_0 = 1.2\ fm$. Considering strong coupling limit, K = J was considered in the present calculation by following Ref. [29].

In Fig. 8, the deformation parameters β_2 have been plotted as a function of N, for few odd-Z and odd-A nuclei around ^{132}Sn. It is observed that the deformation decreases monotonically as one approaches N = 82, establishing the spherical character at shell closure. The deformation for $5/2^+_1$ level of ^{131}I, measured in the present work, also fits closely with the systematics.

4.2 Shell model calculation

The large basis shell model (LBSM) calculations were already performed earlier [20] for ^{131}I nucleus using the code NUSHELLX [30] that considered ^{100}Sn as core. In this calculation, the particles were distributed over the 50-82 subshell valence space comprised of ($1g_{7/2}$, $2d_{5/2}$, $2d_{3/2}$, $3s_{1/2}$, $1h_{11/2}$) single particle orbitals with the single particle energies and interaction matrix elements as given in Ref. [20]. The said calculation was quite successful in interpreting the level energies and transition probabilities in ^{131}I and ^{132}Xe. In the present work, the calculation was extended for the estimation of quadrupole moment of $5/2^+_1$ level in ^{131}I using

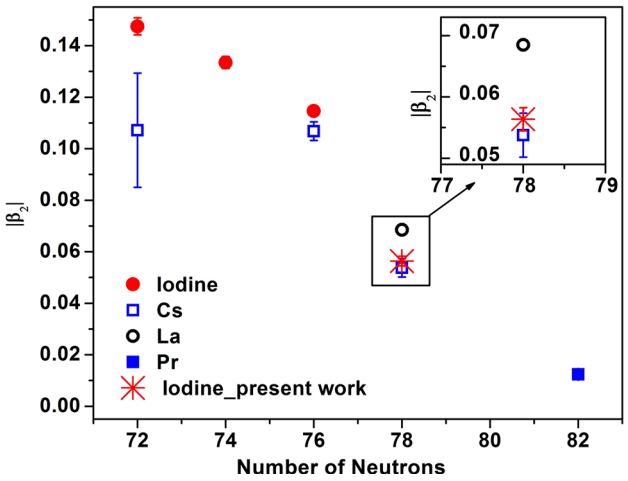

Fig. 8 Deformation (magnitude), as deduced from the experimental quadrupole moments, are plotted with neutron numbers. The experimental quadrupole moments for the $5/2_1^+$ levels of odd-A iodine (I), Cesium (Cs), Lanthanum (La) and Presodymium (Pr) nuclei have been taken from Ref. [6], except that of ^{131}I that is measured in the present work. Errors have been considered but not visible in some cases as the corresponding error bars are smaller than the size of the symbol used. The error is not shown in case of La as it is very high (100%)

the standard effective charges ($e^p = 1.35, e^n = 0.35$), as was also used for the estimation of transition probabilities in Ref. [20].

The calculation estimates a value of -0.34 eb for the $5/2_1^+$ level of ^{131}I that explains quite well the EQM measured in the present work ((−)0.30(1) eb). For ^{132}I, the first excited level was calculated at 75 keV and the spin parities of both the ground state and first excited level could be reproduced from the present calculation. The calculated value for the EQM of 3_1^+ level of ^{132}I, using standard effective charges, comes out to be -0.18 eb which is also close to the experimental data.

The increase in quadrupole moment for the $5/2_1^+$ levels, to a value of -0.761 (17) eb for N = 72 iodine, is observed with the increase in number of neutron hole pairs compared to N = 82 shell closure. This can be understood as due to the admixtures of different configurations to the wavefunction of the $5/2_1^+$ levels and the corresponding increase in collectivity. Such configuration mixing has been studied through measurement of spectroscopic factors for the $5/2_1^+$ levels in odd-A I nuclei through proton transfer reactions [31,32]. However, these data show almost constant spectroscopic factors for the $5/2_1^+$ levels with l = 2 (J = 5/2) and, therefore, similar contribution from the $\pi d_{5/2}$ orbital in the $5/2_1^+$ levels of $^{125-131}$I. This concludes that the sum of admixtures of all other possible particle configurations amounts to be similar for all the $5/2_1^+$ level in these iodine nuclei. So, to understand the experimental observation, it would be interesting to study the admixtures in all these $5/2_1^+$ levels of odd-A iodine isotopes from shell model calculation, as a future perspective to the present work.

5 Summary

The EQMs for the $5/2_1^+$ level in ^{131}I and 3_1^+ level in ^{132}I have been measured using TDPAC method. The present measurement provides the first experimental data for the EQM of the $5/2_1^+$ level in ^{131}I (N = 78) which amonuts to be (−)0.30(1) eb. The quadrupole moment of 3_1^+ level of ^{132}I has also been measured to be (−)0.25(2) eb with a different technique. It is found that a linear interpolation, using the present experimental data and few selected datasets, viz. at N = 72 and 76, predicts the quadrupole moment for the $5/2_1^+$ level as lower than that for $7/2_1^+$ level at N = 82 iodine. The experimental data on nuclear deformation for the $5/2_1^+$ levels in the odd-Z, odd-A nuclei close to ^{132}Sn show a monotonic decrease of deformation up to N = 82, corroborating with the double shell closure of ^{132}Sn. The quadrupole moment for the first excited levels of ^{131,132}I have also been calculated using large basis shell model and are found to closely reproduce the experimental data. It is realized that the experimental measurement at N = 82 and more involved large basis shell model calculations for the N = 72–82 iodine nuclei might be useful to understand the real scenario on the evolution of EQMs up to N = 82.

Acknowledgements The K-130 cyclotron operation group at VECC, Kolkata, is gratefully acknowledged for providing high quality ^{4}He beam. S. S. A acknowledges support from BRNS (Sanction No. 2013/38/02-BRNS/1927 for PRF, BRNS, dated 16 October 2013) towards his PhD fellowship. Mr. R. K. Chatterjee, RCD, VECC is acknowledged for his assistance in target preparation and radiochemical separation. A. S acknowledges the UGC JRF/SRF fellowship (ref. No:17-06/2012(i)EU-V) in support of participation in the present work. Mr. Anish Kar Mahapatra of CMPD, SINP is sincerely acknowledged for carrying out the XRD measurement. D. B thankfully acknowledges Dr. R Acharya, Head, NA & AC Section, RCD, BARC and Dr. P. K. Pujari, AD, RC & I Group, BARC for their kind support in the present work.

Data Availability Statement This manuscript has no associated data or the data will not be deposited. [Authors' comment: The datasets generated during and/or analyzed during the current study are available from the corresponding author on reasonable request.]

References

1. E. Dafni et al., Phys. Rev. Lett **55**, 1269 (1985)
2. B. Hinfurtner et al., Phys. Rev. Lett **67**, 812 (1991)
3. J.M. Allmond et al., Phys. Rev. C **84**, 061303(R) (2011)
4. F. Le Blanc et al., Phys. Rev. C **72**, 034305 (2005)
5. R. Sifi et al., Hyperfine Interact **171**, 173 (2006)
6. N.J. Stone, Atom. Data and Nucl. Data Tables **111–112**, 1 (2016)
7. D.W. Hafemeister, G. Depasquali, H. Dewaardd, Phys. Rev. **135**, B1089 (1964)
8. L.S. Kisslinger, R.A. Sorensen, Rev. Mod. Phys. **35**, 853 (1963)
9. Hisashi Horie, Akito Arima, Phys. Rev. **99**, 778 (1955)
10. Rosalie Robinette, J .G. Cosgrove, R .L. Collins, Nucl. Instr. Meth **105**, 509 (1972)
11. H. Haas, D.A. Shirley, J. Chem. Phys. **58**, 3339 (1973)

12. H. Ooms et al., Nucl. Phys. A **321**, 180 (1979)
13. M. Grodzicki et al., J. Phys. B **20**, 5595 (1987)
14. H. Fraunfelder, R. M. Steffen, Alpha Beta and Gamma Ray Spectroscopy, K. Siegbahn, Ed. Vol II, Chap. XIX , North Holland, Amsterdam(1965)
15. https://www-nds.iaea.org/nuclearmoments/
16. J.P. Adloff, Radiochimica Acta **25**, 57 (1978)
17. T. Butz et al., Nucl. Instr. Meth. Phys. Res. A **284**, 417 (1989)
18. Yu. Khazov et al., Nucl. Data Sheets **104**, 497 (2005)
19. Yu. Khazov, I. Mitropolsky, A. Rodionov, Nucl. Data Sheets **107**, 2715 (2006)
20. S.S. Alam et al., Phys. Rev. C **99**, 014306 (2019)
21. R. Vianden, *Hyperfine Interactions* **15/16**, 1081 (1983)
22. G. Langouche et al., Phys. Rev. B **9**, 848 (1974)
23. P. Pyykkö, Mol. Phys. **116**, 1328 (2018)
24. M. Tanigaki et al., Phys. Rev. C **80**, 034304 (2009)
25. T. Butz, *Fourier Transformation for pedestrians*, **2nd Ed. Springer** pp 71 (2015)
26. S .S. Alam et al., Nucl. Instr. Meth. Phys. Res. A **874**, 103 (2017)
27. P.N. Tandon, H.G. Devare, Nucl. Phys. A **102**, 203 (1967)
28. L.M. Beyer, W.H. Kelly, Nucl. Phys. A **104**, 274 (1967)
29. M. Ionescu-Bujor et al., Phys. Lett. B **650**, 141 (2007)
30. B.A. Brown, W.D.M. Rae, Nucl. Data Sheets **120**, 115 (2014)
31. R.L. Auble, J.B. Ball, C.B. Fulmer, Phys. Rev **169**, 955 (1968)
32. A. Szanto de Toledo, H. Hafner, H.V. Klapdor, Nucl. Phys. A **320**, 309 (1979)